machines

MDPI

*Article*

# Fast Load Distribution Calculation for Cylindrical Gears with Non-Involute Tooth Profiles

**Karsten Fetzer *, Stefan Landler, Jonas-Frederick Berger, Michael Otto and Karsten Stahl**

Gear Research Center (FZG), TUM School of Engineering and Design, Technical University of Munich, Boltzmannstraße 15, D-85748 Garching, Germany; stefan.landler@tum.de (S.L.); jonas.f.berger@tum.de (J.-F.B.); michael.k.otto@tum.de (M.O.); karsten.stahl@tum.de (K.S.)

* Correspondence: karsten.fetzer@tum.de

**Abstract:** Advancements in manufacturing technology provide users with new opportunities for the design of gears. Special gearings with customized non-involute tooth profile geometries offer a promising alternative to conventional involute gears, addressing limitations, such as undercutting and small radii of curvature near the tooth root. However, the absence of standardized design procedures for non-involute gears, such as ISO 6336 for involute gears, often necessitates reliance on numerical simulations and methodologies using approximations. Analytical methods for determining key parameters—such as the topological load distribution and contact pressures—are currently specialized for involute gears and can hardly be directly applied to special gears. This paper proposes a generalization of the analytical static load distribution calculation for non-involute tooth profiles. A relationship between the applied torque and the transmission error at every meshing position is derived. This approach is validated using the calculation software RIKOR with two exemplary involute gearings, demonstrating consistency with the established method. Additionally, the proposed framework is applied to an exemplary cycloid gear and an eccentric cycloid gear to demonstrate the capability to analyze arbitrary tooth profile geometries. The results highlight the potential for the reliable and efficient design of non-involute gears through analytical methods.

**Keywords:** load distribution calculation; non-involute gearings; cycloid gears; eccentric cycloid gears; EC gearing

check for updates

Academic Editor: Hui Ma

Received: 28 November 2024
Revised: 23 December 2024
Accepted: 26 December 2024
Published: 31 December 2024

**Citation:** Fetzer, K.; Landler, S.; Berger, J.-F.; Otto, M.; Stahl, K. Fast Load Distribution Calculation for Cylindrical Gears with Non-Involute Tooth Profiles. *Machines* **2025**, *13*, 22. https://doi.org/10.3390/machines13010022

**Copyright:** © 2024 by the authors. Licensee MDPI, Basel, Switzerland. This article is an open access article distributed under the terms and conditions of the Creative Commons Attribution (CC BY) license (https://creativecommons.org/licenses/by/4.0/).

## 1. Introduction and State of the Art

Gears are widely used machine elements for transmitting power. A targeted design is necessary to maximize the efficiency, power density, and lifespan of machines and their parts. For involute gears, ISO 6336 [1] is the standard to determine the load capacity in the design process. Safety factors are determined to account for the different damage types of gears. For several damage mechanisms, the load distribution and contact pressures occurring on the tooth flank are the essential parameters. Therefore, multiple methods were developed to calculate the topological distribution of the applied load on the tooth flank, based on different analytical, hybrid, or numerical approaches. Prior to the application of most analytical methods is the determination of the tooth stiffness. Weber and Banaschek [2] (W/B) derive three analytical formulae to calculate the tooth stiffness for an involute spur gear with an infinite width, based on substitute mechanical models of a loaded linear elastic beam and a loaded elastic half-plane. The total deflection of a mating tooth pair is divided into three parts: contact deformation, tooth bending, and tooth tilting. These parts are independently calculated and added together. The final equations are

derived under the assumption of planar strain and for the specific steel material. Geiser and Schinagl [3] validate this approach with a numerical finite element simulation and experimental measurements of the deformation of a spur gear in a pulsator test rig. They find good agreement of the theory with the simulation and measured deformations. Lutz [4] extends this approach to a planar stress assumption and different materials. Hochrein et al. [5] derive the equations of W/B in a closed formulation for both planar stress and planar strain assumptions and consider a better influence coefficient for the shear deformation. They validate the analytical approach with a finite element study without considering the influence of the contact deformation. Even the standardized approach to determine the theoretical tooth stiffness for involute gears with a standard rack tooth profile, as defined in ISO 6336 [1] and DIN 3990 [6], is based on the analytical framework of W/B.

A substitute model of the gear is commonly used to calculate tooth stiffness for varying contact points on the tooth flank. The gear is divided into thin uncoupled slices in its width direction, and for every gear slice, the tooth stiffness is calculated according to the W/B approach [7]. Lutz [4] uses this uncoupled approach on worm gears. Schmidt [8] introduces the coupling of the gear slices with a mechanical model of a finite cantilever plate loaded at the edge. The plate stiffness is calibrated using the W/B approach.

A hybrid approach can also determine the deformation of coupled gear slices under loads. Often based on different numerical simulations, an analytical formulation is derived. In a finite element study, Kunert et al. [9] determine a general relative coupling function for spur gears with an infinite width. They also extend the method to finite gears and are able to consider the influence of free surfaces. Schaefer [10] adapts the coupling functions for bevel gears and Wu [11] for skew involute gears.

Apart from the analytical and semi-analytical approaches, numerical calculations of the load distribution and tooth stiffness are also widely used. Marafona et al. [12] give a general gear mesh stiffness calculation overview. Natali et al. [13] focus more on finite-element-based methods for mesh stiffness calculations.

Based on the determined tooth pair's stiffness and the stiffness of single gear slices, the load distribution on the tooth flanks can be analytically calculated. Placzek [14] derives a set of linear equations with influence coefficients based on a mechanical substitute model of springs and wedges. This approach can model the complete elastic gearbox system consisting of a gear stage, shafts, bearings, and the housing and can also consider non-load-dependent deflections, like tooth modifications. The software program RIKOR is based on this theory and analyses the tooth contact of involute gears in arbitrary load cases and the design of topological tooth modifications [15,16]. Daffner [17] validates the approach of RIKOR with measurements of real gearboxes under loads.

As the widely used standard gear profile geometry, the mentioned calculation approaches are often formulated explicitly for involute gears. However, advancements in manufacturing have made non-involute gearings a viable alternative to involute gears, with the possibility for overcoming certain limitations, like undercutting and small radii of curvature near the tooth's root. Innovative manufacturing techniques, such as five-axis milling [18] and additive manufacturing [19], open up new possibilities for economically and precisely producing special gears.

The freedom to design new gear geometries specialized for specific applications is limitless. Johann and Scheurle [20] derive a set of differential equations based on the law of gearing to determine the geometry of any mating gear profile from a defined tooth flank geometry or a line of contact. Römhild and Linke [21] overview different involute and non-involute special gears. Historically, the cycloid gear plays an important role. Lehmann [22] describes the geometries of cycloid and trochoid gears. A further evolution of the cycloid gears is the eccentric cycloid (EC) gear. Landler et al. [23] derive a parameter-

based definition of them. Kazakyavichyus et al. [24] determine the contact pattern of a single-toothed arc pinion and investigate the influence of deviations from the center distance on the engagement. The geometry of the same EC gearing (single-toothed arc gear) is described by Li et al. [25] as well. They further study the undercutting conditions and the tooth contact and, respectively, the contact lines and surface of action. Furthermore, a loaded-tooth contact analysis is numerically performed with a finite element simulation. Batsch et al. [26] apply micro-modifications to the tooth flank of an EC gearing and study the transmission error.

A mathematical description of a profile cutter to manufacture EC gearings is shown by Bubenchikov et al. [27]. Batsch manufactured a multiple-toothed EC gearing via additive manufacturing [28].

For the targeted and reliable design of non-involute tooth profiles, numerical approaches are often employed to determine key parameters for the load capacity calculation. Specialized methods developed for involute gears are usually not directly applicable, and the absence of standardized methods increases the effort required to design non-involute gears. Therefore, the adaptation of analytical methods to determine key parameters for damage mechanisms and safety factors for special gears would be desirable.

As a first step to address this challenge, this paper proposes a generalization of the analytical load distribution calculation for general non-involute tooth profiles.

## 2. Methods

### *2.1. Generalized Analytical Load Distribution Calculation*

To perform an analytical calculation of the load distribution of involute cylindrical gears, a spatial discretization of the contact surface is necessary. A practical approach is investigating a finite number of meshing sequences and a contact path's discretization at one meshing position in the gear's width direction. The finite points on the contact surface can further be mapped to the corresponding contact points on the tooth flanks of the two mating gears. The discrete points of the contact lines can be determined analytically through a load-free contact analysis. An analytical description of the tooth flank geometry and the field of contact of the investigated gearing is, therefore, beneficial. The number of teeth in contact and the discretized lines of contact at every meshing position serve as input to the analytical load distribution calculation. By conducting a stationary analysis, by applying the load quasi-statically and assuming no change in the position of the calculated contact points because of small deformations, the load distribution calculation results in solving a linear set of equations. For the following derivations, a frictionless contact is assumed.

For involute cylindrical gears, the analytical method is based on Placzek's two-dimensional model for every meshing position [14]. Considering the planar geometry of the plane of action, the global deformation of all the mating tooth flanks in contact at one meshing position is assumed to be constant in magnitude and direction. Including possible non-load-dependent local modifications of the tooth flanks ($\delta_i^*$) in the equations, a set of linear equations for all the contact points can be derived relating the local normal contact forces ($F_{bn,i}$) and the resulting normal displacement ($\delta_{ges}$) via the local stiffnesses ($c_{ij}$) at every point. The local normal forces have to be in equilibrium with the applied torque ($T$) related to the radius of the base circle ($r_b$) of one gear and multiplied by the inverse of the cosine of the base helix angle ($\beta_b$). Summing up over all the finite local forces, one linear equation can be obtained, which can be solved for the resulting displacement ($\delta_{ges}$) in the plane of action as follows [14,29]:

$$\frac{T}{\cos(\beta_b) r_b} = \sum_{i=1}^{n} F_{bn,i} = \sum_{i=1}^{n} \sum_{j=1}^{n} c_{ij} \left( \delta_{ges} - \delta_i^* \right). \quad (1)$$

The resulting global displacement ($\delta_{ges}$) can also be interpreted, when related to the radius of the base circle ($r_b$) of one gear, as the transmission error at this specific meshing position under the particular load case. With the magnitude of the resulting displacement, the local normal contact forces can be calculated via a simple vector–matrix multiplication with the stiffness matrix.

For cylindrical conjugated gears with a general non-involute tooth profile, the field of action is generally not planar but curved. Therefore, the local pressure angles at the contact points of the mating tooth pairs at one meshing position differ typically. Considering an exemplary cycloid gear, the normal vectors ($n_{CP1}$) and ($n_{CP2}$) for two points in contact of the driving gear at one meshing position in the transverse plane are schematically represented in Figure 1. The local normal deformation due to the contact forces is in the same direction as the local normal vectors. Obviously, the directions of the normal vectors differ, and, therefore, no uniform global displacement vector at the meshing position can be assumed. The approach of Placzek [14] is not directly applicable to general non-involute teeth. The pitch point (C) is marked on the line of action in Figure 1.

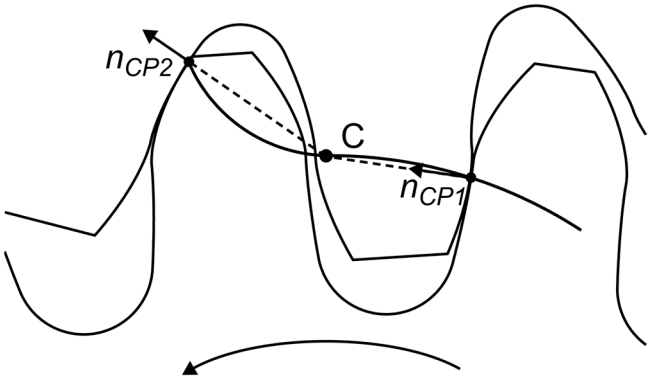



**Figure 1.** Different normal vectors of two contact points on the driving gear's flank at one exemplary meshing position of a cycloid gearing. The driving gear is marked with an arrow indicating the direction of rotation. The dashed lines connecting the contact points to the pitch point highlight the differing directions of the normal vectors at the contact points.

To make the analytical load distribution calculation accessible for general conjugated non-involute tooth profiles of cylindrical gears, a formulation other than that of a normal force–global normal displacement relation has to be derived. Similar to the approach of Placzek [14] for involute gears, the number of teeth in contact and the discretized lines of contact serve as inputs to the calculation method. An analytical description of the tooth flank geometry and the field of action of the investigated gearing is, therefore, beneficial. The idea is to deduce a relation between the applied torque ($T$) and the resulting global angle of displacement ($\varphi_{ges}$) due to the elastic deformation of the tooth flanks.

Kinematically, the separation of the local normal deflection at every contact point ($\delta_{n,i}$) into its transverse and axial components is suggested. Therefore, the local base circle's radius ($r_{b,i}$) is introduced as the lever arm of the force acting on the contact point in the normal direction related to the gear's center. At this radius, the local helix angle ($\beta_{b,i}$) can be used to separate the normal deflection in its transverse direction. The angle $\beta_{b,i}$ is called the local base helix angle and the distance $r_{b,i}$ is the local base radius, following the conventions for involute gears. The transverse displacement ($\delta_{t,i}$) is assumed to be the arc

length of the global deformation angle ($\varphi_{ges}$) at this meshing position, with the local base circle's radius ($r_{b,i}$) of the contact point. Thus, the angle is related to one gear of the stage.

The angle $\varphi_{ges}$ can also be interpreted as the transmission error of the gearing in the meshing position. The local normal displacements are associated with the global deformation angle through the following equation:

$$\varphi_{ges} = \frac{\delta_{t,i}}{r_{b,i}} = \delta_{n,i}\frac{cos(\beta_{b,i})}{r_{b,i}} \,. \tag{2}$$

Figure 2a presents a schematic cycloid gearing in the transverse plane. The driving gear is loaded with an applied torque in the positive z-direction. Under the load, the gear teeth deform on contact. The deformed gear teeth are schematically represented with dotted lines. The relation and definition of the local transverse deflection ($\delta_{t,i}$) of the contact point (CP), the local base radius ($r_{b,i}$), and the global deformation angle ($\varphi_{ges}$) are depicted. In Figure 2b, a schematic of a helical gear's finite gear slice with its transverse width ($b_t$) is shown in a planar view. The deformed tooth trace is marked with a dashed line. The torque is applied in the positive z-direction. The relation of the normal force and displacement with the corresponding quantity in the transverse direction via the local base helix angle ($\beta_{b,i}$) at the contact point (CP) is presented. Additionally, according to the thin slice model [7], the corresponding width ($b_n$) of the gear slice, perpendicular to the normal direction, is shown.

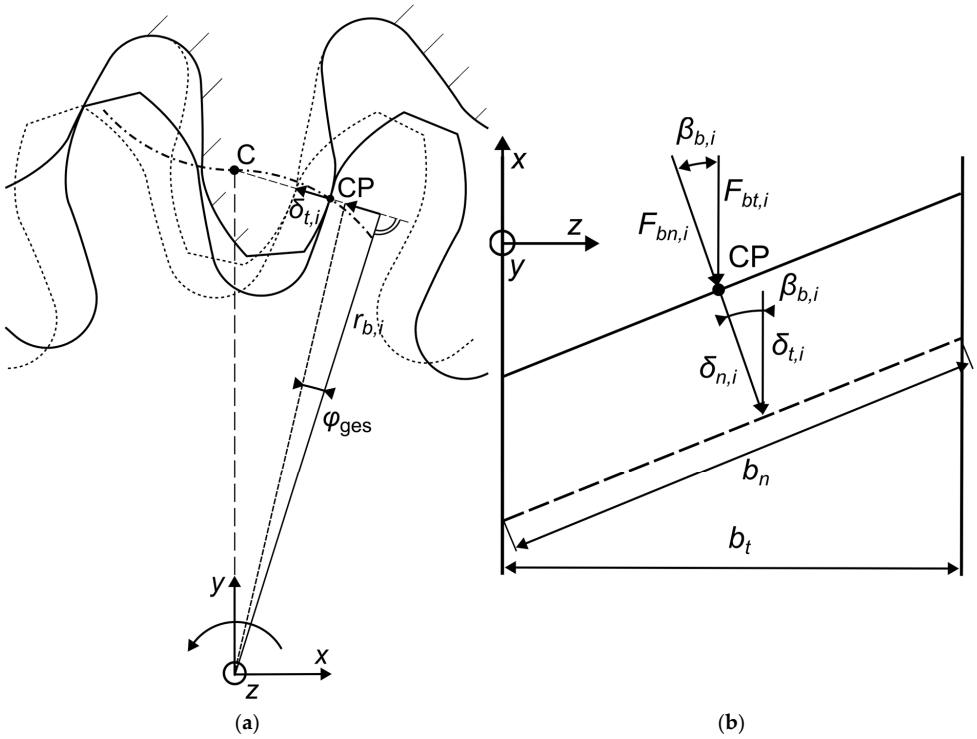



**Figure 2.** (**a**) A schematic representing the relation between the deformation angle and the transverse deflection of a cycloid gear. The pitch point (C) is marked on the dashed line of contact. The driving gear is loaded with a torque in the positive z-direction, as indicated by the arrow at the frame of reference. The mating gear is fixed, represented by the hatched pattern. Under the load, the teeth in contact deform, as indicated by the dotted lines, resulting in a rotational displacement of the driving gear by the angle $\varphi_{ges}$. (**b**) Planar view schematic representing the local relationship between the normal force and deformation, and the corresponding transverse quantity at the contact point of a helical gear in the normal direction. The torque is applied in the positive z-direction, and the deformed tooth trace is marked with a dashed line.

In a quasi-static frictionless analysis, the externally applied torque ($T$) is always in static equilibrium with the resulting normal line loads along the contact lines. In the discretized model, local normal force ($F_{bn,i}$) acts on the finite contact points as a resultant of the corresponding normal line load integrated over the finite gear width between two contact points. The static equilibrium can then be written as follows [29]:

$$T = \sum_{i=1}^{n} F_{bt,i} r_{b,i} = \sum_{i=1}^{n} F_{bn,i} r_{b,i} \cos(\beta_{b,i}) \, . \tag{3}$$

The local normal forces ($F_{bn,i}$) are in a relation with the local forces projected in the transverse direction ($F_{bt,i}$) and the cosine of the local helix angle ($\beta_{b,i}$) at every contact point, as can be seen in Figure 2b. The transverse forces ($F_{bt,i}$) multiplied by the local base radius ($r_{b,i}$) and summed up over all the contact points results in the applied torque.

The kinematics (Equation (2)) and global equilibrium (Equation (3)) can be linked with an appropriate constitutive relation modeling the gear's behavior under static loads. Assuming a linear elastic behavior, the resulting normal deformation due to a normal force at a discrete point on the tooth flank can be calculated using the stiffness matrix ($c_{ij}$). Inserting relationships (2) and (3) into the expression of Equation (1) and substituting the normal deflection ($\delta_{ges}$) in Equation (1) with the resolved expression for the local normal deflections ($\delta_{n,i}$) from Equation (2) results in

$$T = \sum_{i=1}^{n} \sum_{j=1}^{n} c_{ij} \left( \varphi_{ges} r_{b,i} \frac{1}{\cos(\beta_{b,i})} - \delta_i^* \right) \cos\left(\beta_{b,j}\right) r_{b,j} \, . \tag{4}$$

This linear equation can be solved for the global deformation angle ($\varphi_{ges}$) at every discretized meshing position. With the angle $\varphi_{ges}$, the local normal contact forces can be calculated with the resulting local deformations for every point in contact and the stiffness matrix. When related to the corresponding gear slice width ($b_n$), the local normal line load and contact pressure can be derived in the next step. According to the approach proposed by Linke et al. [29], the axial width of the gear slice ($b_t$) is modified with the local base helix angle ($\beta_{b,i}$) as follows:

$$b_n = \frac{b_t}{\cos(\beta_{b,i})} \, . \tag{5}$$

The corresponding widths for one gear slice are illustrated in Figure 2b. It has to be pointed out that because of the varying base helix angles ($\beta_{b,i}$) for different contact points, the derived normal gear slice width ($b_{n,i}$) is not constant and, therefore, influences the calculated local contact line load and contact pressure. For involute gears, the angle $\beta_{b,i}$ is constant at every contact point.

The resulting local normal line load ($q_{n,j}$) at a contact point ($j$) can be calculated as follows:

$$q_{n,j} = \sum_{i=1}^{n} c_{ij} \left( \varphi_{ges} r_{b,i} \frac{1}{cos(\beta_{b,i})} - \delta_i^* \right) \cdot \frac{1}{b_{n,j}} \, . \tag{6}$$

Equation (4) has to be solved iteratively for existing local non-load-dependent modifications of the tooth flanks ($\delta_i^*$) and possible non-linearities in the contact deformation's stiffness. The iterative procedure is the same as the well-known analytical method for involute gears, as described in [14]. It is, therefore, possible to calculate the load distribution for tooth geometries with applied micro-modifications, such as axial or longitudinal crowning. The topological modifications have to be determined pointwise in the local normal direction of the contact point and are introduced to the equation as $\delta_i^*$.

In Equation (4), the expression of the stiffness matrix can also be interpreted as a torsional stiffness. Points of contact with a different local base circle radius ($r_{b,i}$) have a

different torsional stiffness and, thus, a different influence on the resulting deformation angle ($\varphi_{ges}$).

Furthermore, a general remark on the stiffness matrix and its coupling coefficients must be made. The off-diagonal terms of the compliance matrix ($c_{ij}^{-1}$) relate an applied normal force at contact point $i$ with a displacement in the normal direction at the point $j$. For general non-involute tooth profiles, the two normal directions of the different contact points on one tooth flank at one meshing position differ from another. Thus, special consideration is necessary when applying analytical calculation methods to determine the compliance matrix and cross-influence, such as Schmidt's method for involute cylindrical gears [8], and possible adaptations must be made.

The needed stiffness matrix ($c_{ij}$) for the presented calculation method can be analytically derived using well-established approaches [5,8] or using numerical simulation techniques. A fast and profile-geometry-independent approach offers a fully analytical tooth stiffness calculation. The twist of a finite helical gear slice is neglected [29], and a representative two-dimensional normal cross-section of the cylindrical gear needs to be determined for modeling the tooth's stiffness in the load case. An established choice of the planar normal cross-section exists for involute gears, with good practical results. To apply the derived analytical load distribution calculation method to general tooth profiles, a simplified generalized definition of a representative planar normal cross-section is necessary.

### *2.2. Planar Normal Cross-Section of the Tooth Profile for the Analytical Tooth Stiffness Calculation*

For involute gears, various conventions exist for a two-dimensional tooth's normal cross-section. An easy and practical approach is to adjust the profile's tooth thickness in the transverse cross-section ($s_t$) with the gear's helix angle ($\beta$) [29]. For every contact point and every gear slice, the twist of the helical gear is neglected. The tooth profile is substituted with an equivalent spur gear with a width of $b_n$, and the tooth thickness ($s_n$) is calculated using the helix angle ($\beta$).

In this case, for defining a representative normal cross-section for general non-involute cylindrical gears, the same approach for modifying the profile's transverse tooth thickness by the cosine of a helix angle is used. To consider the varying contact points on the tooth profile, the local helix angle ($\beta_{y,i}$) at one contact point is suggested to be used. It varies from the tooth tip to the root. This approach picks up the idea of the established tooth thickness adaption for involute gears and generalizes it to consider the local position of the contact point on the tooth flank. For non-involute tooth profiles, the angle $\beta_{y,i}$ can be analytically calculated at every contact point on every tooth flank. The transverse tooth thickness ($s_{t,i}$) is modified to obtain the thickness of the representative normal cross-section ($s_{n,i}$). Equation (7) presents the relation between the tooth thicknesses of the different cross-sections:

$$s_{n,i} = s_{t,i} cos(\beta_{y,i}) . \tag{7}$$

The gear's width ($b_{n,i}$) of the equivalent spur gear slice is calculated using the previously introduced Equation (5).

The proposed convention of a representative cross-normal section differs from the normal section's definition in DIN ISO 21771 [30]. This is because the norm's definition results in a curved shape of a normal profile and is, thus, not planar [31]. The simplified convention neglects this and proposes an alternative approach motivated by the well-established definition for involute gears. Both planar normal cross-sections do not consider changes in the tooth's height and symmetry when intersecting the gear's tooth in a plane normal to the tooth traces and containing the flank's normal vector at the contact point.

Often, the local angles ($\beta_{y,i}$) only slightly differ for various contact points. Consequently, the difference between the resulting normal cross-sections is small, and as a further simplification, a uniform normal cross-section of the tooth profile can be suggested. One representative contact point is chosen, and the corresponding normal cross-section of the tooth profile at this specific point is used for further calculations. The other contact points must be projected onto the normal geometry, and the corresponding normal vectors must be determined, for example, through numerical methods.

## 3. Results and Discussion

### *3.1. Comparative Calculation with RIKOR*

To validate the proposed method, a comparison with the calculation software RIKOR is carried out. RIKOR is a specialized calculation and design program for involute gears. Therefore, two exemplary involute gearings are investigated, and the load distribution and transmission error for both calculation methods are compared. The specific gear parameters are listed in Table 1. No micro-modifications of the tooth flanks are applied to the gears.

**Table 1.** Characteristic gear parameters used for comparative calculation. Names are according to DIN ISO 21771 [30]. All the length-related parameters are referenced in millimeters (mm). All the angle-related parameters are given in degrees (°).

| *No.* | $z_1$ | $z_2$ | $\alpha_n$ | $x_1$ | $x_2$ | $m_n$ | $a$ | $b$ | $\lvert\beta\rvert$ | $d_{Na1}$ | $d_{Na2}$ | $d_{Nf1}$ | $d_{Nf2}$ |
|---|---|---|---|---|---|---|---|---|---|---|---|---|---|
| 1 | 30 | 40 | 20 | 0 | 0 | 3 | 105 | 25 | 0 | 94.20 | 124.20 | 86.85 | 116.77 |
| 2 | 30 | 40 | 20 | 0 | 0 | 3 | 108.7 | 25 | 15 | 97.37 | 128.43 | 89.94 | 120.93 |

For the comparison, an external torque of $T = 70$ Nm is applied to the first gear of the stage for both investigated gearings. The material of all the gears is steel and modeled as linear elastic and isotropic, with a Young's modulus of $E = 210$ GPa and a Poisson's ratio of $\nu = 0.3$.

For the calculation of the stage's stiffness, the influences and elasticities of the shafts, bearings, and housing are not modeled, and all the parts except for the gearing itself are assumed to be ideally stiff. The stiffness of the gearing itself is calculated in the presented approach with the analytical method presented by Hochrein et al. [5]. The influence of the contact deformation is modeled using the same approach as Weber and Banaschek [2]. Because of the non-linearity of the contact deformation, the iterative solving procedure has to be applied [14]. In the used stiffness calculation method, no cross-influence, for example, as proposed by Schmidt, with a substitute model of a finite cantilever plate [8], is considered. The finite gear slices deform independently from one another, and the stiffness matrix has only diagonal elements. This method induces an error but is sufficient to calculate the load distribution of general conjugate gears and to compare the presented approach with RIKOR. However, an overall overly compliant behavior of the gears in the presented method is expected due to neglecting the coupling between gear slices in the stiffness modeling. Additionally, premature teeth meshing and boundary effects at the free surfaces and the tooth tip are not modeled either. Deviating results in this area are to be expected to a certain extent.

The load-free, frictionless contact analysis of the presented gearings is determined analytically and used as input for the calculation approach. The tooth root's geometry in the presented calculation approach is modeled as a circular fillet with a tangential transition. The tooth flank is modeled with 130 finite points, and the gear's width is discretized with 100 thin slices. The width's discretization influences the results only for helical gears because of the used substitute model of finite gear slices. To determine the load distribution

on the tooth flank, 100 individual meshing positions are investigated. The planar normal cross-section for every contact point is modeled with the approach presented in Section 2.2.

In RIKOR, the tooth width is discretized with 100 finite points, and 100 different meshing positions are evaluated for the load distribution. The transmission error is calculated at 50 individual meshing positions for one periodic meshing sequence. The shafts, bearings, and housing are modeled to be ideally stiff. No premature tooth meshing is considered. The stiffness calculation method used in RIKOR is based on the approach by Schmidt [8].

#### 3.1.1. Comparison for an Exemplary Spur Gear (Gearing No. 1)

The calculated transmission errors (TE) of gearing no. 1 (Table 1) in this specific load case are plotted in Figure 3 for both calculation methods. For the proposed approach, the general computed angle of deflection ($\varphi_{ges}$,) related to the first gear is converted to the transmission error along the path of action, with the constant base circle radius ($r_{b1}$). The error is shown along the contact path, indicating specific points in the meshing sequence. The starting point of the meshing is marked as A. In the interval from A to B, dual-flank engagement is present, and from B to D, single-flank engagement is present. The points B and D each mark the end of the specific engagement. The total contact ratio of the presented gearing is $\varepsilon_\gamma = 1.23$. The resultant curve of the transmission error in Figure 3 is continued periodically until the end point of the meshing.

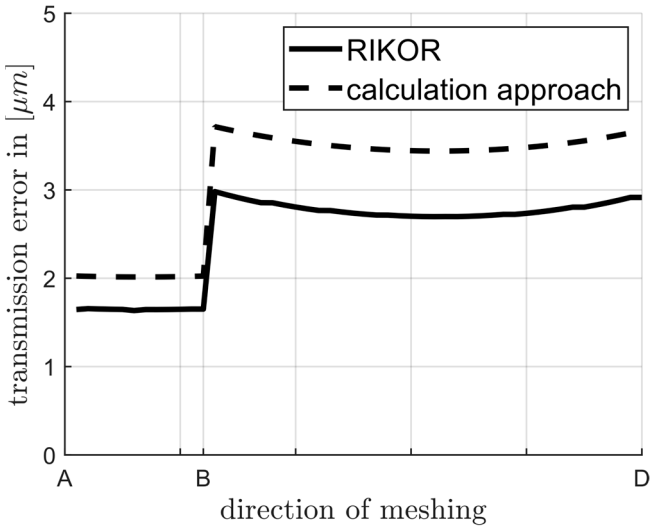



**Figure 3.** Comparison of the transmission errors along the path of contact of gearing no. 1 between the presented calculation approach and RIKOR.

In Figure 3, the calculated TE of the proposed approach is of the same order of magnitude as the reference solution with RIKOR and follows its trend. The shape and curvature of the reference curve are accurately followed in the intervals from A to B and from B to D. The discontinuity at the endpoint of the single-flank engagement (B) is evident in both curves. Nevertheless, the difference in absolute values is visible and almost constant. In the section of the dual-flank engagement (from A to B), the absolute difference between the computed TEs is smaller than in the interval from B to D. The deviations in the calculated tooth stiffness for both contact points of the two meshing tooth pairs partially cancel out, reducing the overall error in this section.

The resulting load distribution obtained using the calculation software RIKOR in this load case is plotted on the field of action in Figure 4a. For the proposed calculation approach, it is depicted in Figure 4b. The color scale is adjusted, and the range of the line load is limited to 25 $\frac{N}{mm}$ up to 70 $\frac{N}{mm}$ for both figures. The differences in the load occurring

on the tooth flank are visible in both figures. During dual-flank engagement, the load is distributed on two gear teeth, whereas in single-flank engagement, the external force acts entirely on one line in contact with the two mating flanks. The end-points, B and D, of the flank engagement sections in Figure 3 can also be identified in Figure 4a,b by the discontinuities in the load distribution.

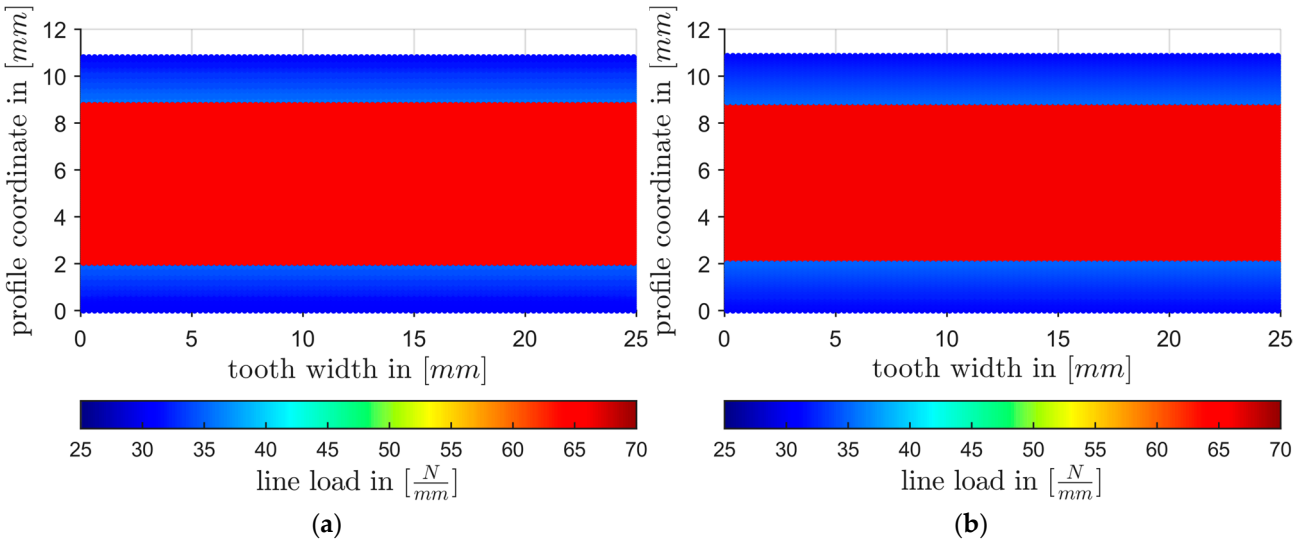



**Figure 4.** Calculated distributions of the line load on the field of contact of gearing no. 1 with (**a**) RIKOR; (**b**) the presented approach.

The load distributions depicted in Figure 4a,b are very similar in the overall shape and order of magnitude. To compare the resulting line loads obtained using the proposed approach ($q_{CA}$) and the calculation software RIKOR ($q_{RI}$) at one specific point relative to each other, the relative deviation is determined as follows:

$$\Delta = \frac{q_{CA} - q_{RI}}{q_{RI}} . \tag{8}$$

Because of the different discretization schemes of the contact lines, a linear interpolation method is used. The finite points of the calculated load distribution obtained from RIKOR are linearly piecewise interpolated and evaluated at specific discrete points in Figure 4b. The relative deviation is evaluated at the particular points plotted in Figure 4b. The indicated scale is limited to values between $-10\%$ and $+10\%$.

As shown in Figure 5, the relative deviation is relatively small in a large region of the field of contact and below 5%. At the starting point of the meshing, the deviation increases. The determined line load in the single-flank engagement is nearly identical, with a relative deviation of only a small percentage. The discontinuity between the different flank engagement sections is not precisely met because of different discretization methods of the plane of action. Overall, the load distribution calculated with the presented approach has good accuracy compared to the results obtained from RIKOR. Considering the deviations in the transmission error along the path of contact in Figure 3, it can be stated that only the relative tooth stiffness at different contact points determines the resulting load distribution of the tooth's flank. Therefore, the differences in the stiffness calculations are, to an extent, irrelevant if the relative stiffness values remain unchanged and only the absolute values differ. The tooth stiffness's absolute values at different contact points are important for the transmission error calculation.

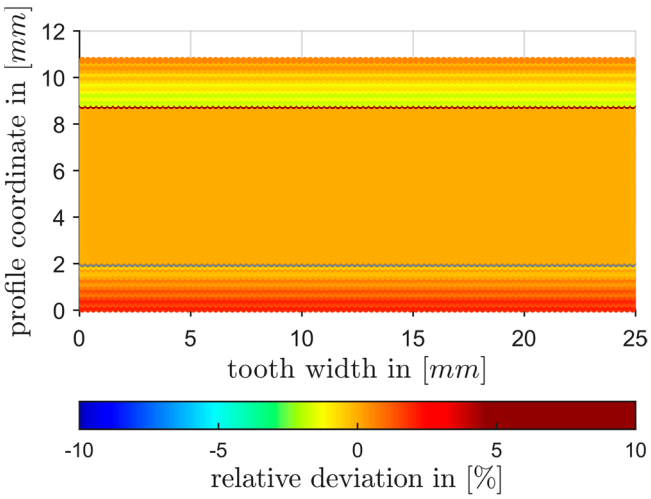



**Figure 5.** Relative comparison of the load distributions of gearing no. 1 between the presented approach and RIKOR according to Equation (8).

#### 3.1.2. Comparison for an Exemplary Helix Gear (Gearing No. 2)

Helical gearing no. 2, according to Table 1, is chosen for the second comparison. The calculated TEs for the specific load case are plotted in Figure 6. Like in Figure 3, the calculated deformation angle ($\varphi_{ges}$) is converted with the base circle radius ($r_{b1}$) to the corresponding TE along the path of action. Important points along the meshing sequences are indicated on the axis. The meanings of the letters remain unchanged in comparison to those in Figure 3. The total contact ratio of gearing no. 2 is $\varepsilon_\gamma = 1.85$. In the interval A–B, dual-flank engagement occurs, and from B to D, single-flank engagement occurs. The plotted TEs are periodically continued until the end of the meshing. The non-smooth behavior of the calculated curves is because of the discretization errors of the contact lines.

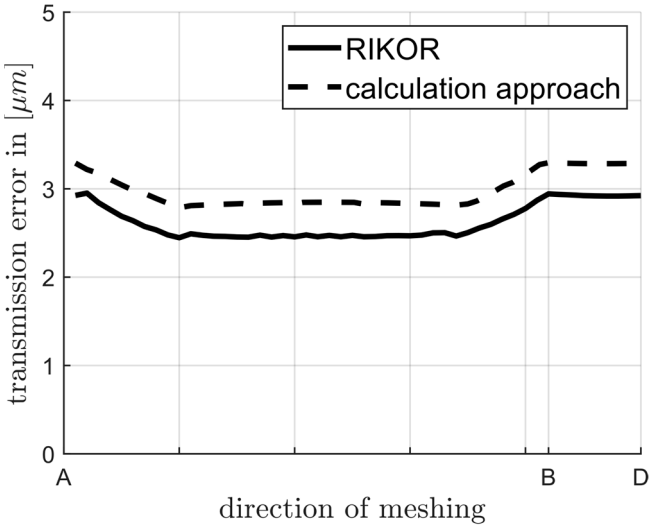



**Figure 6.** Comparison of the transmission errors along the contact path of gearing no. 2 between the presented calculation approach and RIKOR.

As shown in Figure 6, the TE obtained with the proposed approach closely follows the trend of the reference solution determined with RIKOR. For both methods, the TE in the dual-flank engagement interval is lower than that in the single-flank engagement interval. The overly compliant behavior of the proposed method is still apparent, and the determined TE is constantly positioned above the reference solution. The absolute

deviation between both TEs is smaller compared to that obtained for gearing no. 1, as shown in Figure 3.

The line load distributions determined with both approaches are shown on the field of contact in Figure 7a,b. The color scale, representing the line load's value, is identical in both figures and limited from 40 $\frac{N}{mm}$ to 70 $\frac{N}{mm}$. The contact lines proceed from the starting point of the meshing in the bottom left corner to the top right and are diagonal across the field of action.

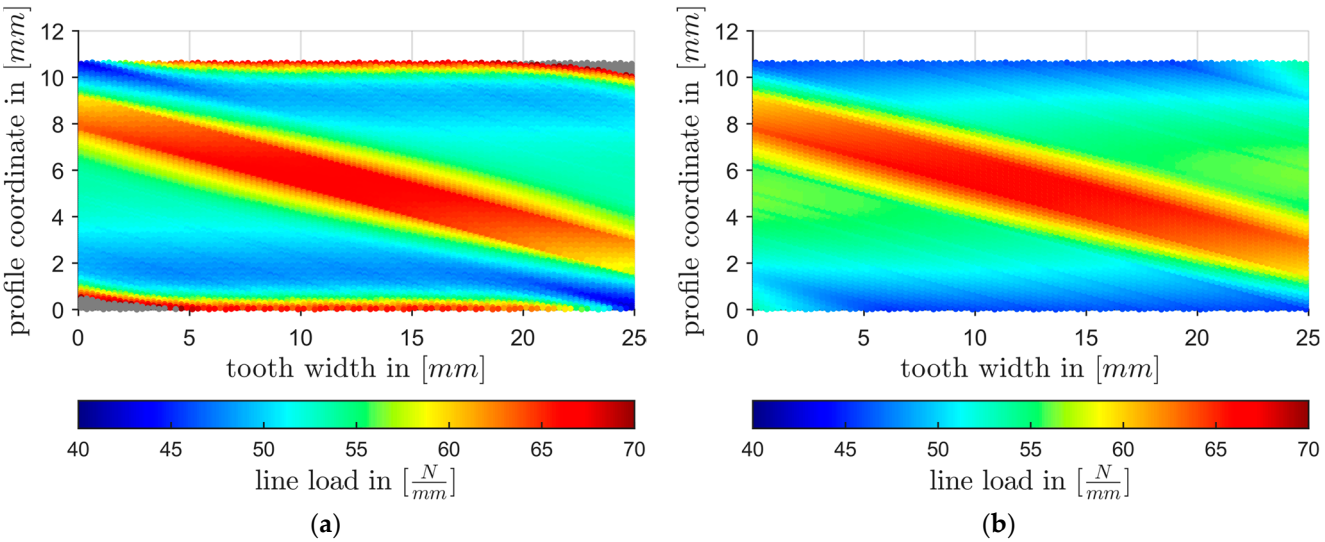



**Figure 7.** Calculated line loads on the field of contact of gearing no. 2 for (**a**) RIKOR; (**b**) the presented approach. The color scale is limited. Outliers are marked gray.

For the reference solution, calculated with RIKOR, a significant increase in the line load toward the tooth tip and root at the ending and starting points of the meshing is visible. The line loads exceed the limited scale and are marked as gray. This can be attributed to the influence of boundary effects on the tooth stiffness. The simplified stiffness calculation used for the presented approach does not capture these effects. Apart from the differences at the tooth tip and root, the field of action is mainly loaded in the middle of both figures. The single-flank engagement interval shows a higher loaded section in this region.

The relative deviation between both load distributions, shown in Figure 8, is calculated in the same way as for gearing no. 1, using Equation (8). The deviation is dominated by the differences at the tooth tip and root near the starting and ending points of the meshing. To better evaluate the relative deviation in the middle of the profile, the color scale is limited to $-10\%$ up to 10%. Outliers are marked gray.

Analyzing the relative deviation between both calculation approaches shows that the determined line load only differs under an absolute of 10% of the reference solution in a wide range of the flank. The determined line load in the single-flank engagement section is in good agreement with the reference solution. As mentioned before, the boundary effects at the tooth tip and root are not captured in the used calculation approach, and the relative deviation is significant in these regions. The higher line loads at the tooth tip and root also influence the loads at the other contact points on the contact's lines at these meshing positions. Therefore, the higher deviations and overestimation of the occurring load in the middle section of the field of contact can be partially explained.

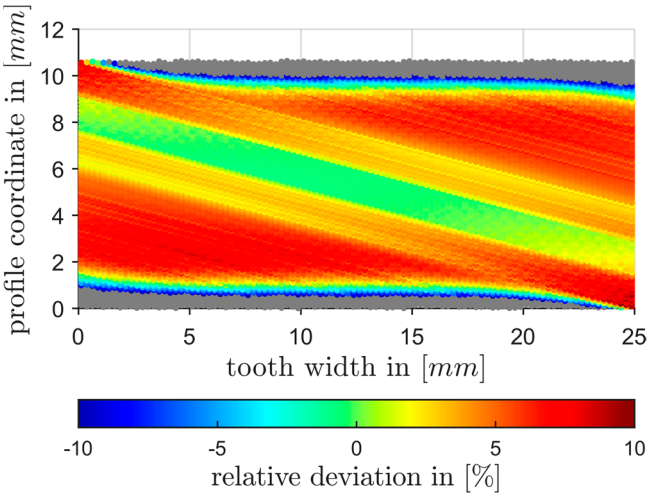



**Figure 8.** Relative comparison of the determined line loads of gearing no. 2 between the presented approach and RIKOR with a limited scale. Outliers are marked gray.

It can be concluded that the proposed calculation approach achieves good results in comparison with RIKOR for both investigated gearings. Despite the different tooth stiffness approaches, the determined line load distribution matches in both cases in good agreement with the results from the reference solution in a large area of the field of contact and relatively deviates under an absolute value of 10%. Better results can be achieved using more sophisticated approaches to analytically calculate the tooth stiffness or using numerically determined results. Boundary effects, for example, can be included in the stiffness calculation method by adopting, e.g., Schmidt's substitute model of a finite cantilever plate [8]. The primary objective of this paper is to validate the proposed approach for involute gears and demonstrate its transferability to non-involute profiles. Therefore, the deviations of the load distribution and TE obtained with the proposed approach compared with those obtained with RIKOR are acceptable.

### *3.2. Application of the Presented Calculation Approach to Non-Involute Tooth Profiles*

One exemplary cycloid gearing and one eccentric cycloid (EC) gearing are used to demonstrate the applicability of the proposed calculation approach to non-involute tooth profiles. The parameterized geometry of the EC gearing is according to Landler et al. [23], and the specific gear parameters are listed in Table 2. The cycloid gearing's geometry is based on that proposed by Lehmann [22]. The gear parameters are shown in Table 3. A circular fillet connects the teeth for both gearings, and the profiles are discretized with 100 points. The design of the gears is similar to that of the investigated involute helix gear (gearing no. 2 in Table 1) in Section 3.1. The same transverse module ($m_t = 3.10$), gear width ($b$), helix angle ($\beta$), load case ($T = 70$ Nm on the first stage), and material assumption (linear elastic, isentropic material with a Young's modulus of $E = 210$ GPa and a Poisson's ratio of $\nu = 0.3$) are used. The tooth height is chosen similarly. A comparison of the transverse teeth profiles can be seen in Figure 9a for the pinion and in Figure 9b for the mating gear.

**Table 2.** Gear parameters of the investigated EC gearing according to Landler et al. [23]. All the length-related parameters are referenced in millimeters (mm). All the angle-related parameters are given in degrees (°).

| $z_1$ | $z_2$ | $a$ | $\beta$ | $b$ | $\lambda$ | $\varphi_{A,s}$ | $\varphi_{A,e}$ | $r_a^*$ | $S_t^*$ | $c^*$ | $\varphi_j$ |
|---|---|---|---|---|---|---|---|---|---|---|---|
| 30 | 40 | 109.80 | 15 | 25 | 0.99 | 0 | 180 | 1 | 1 | 0.1 | 0 |

**Table 3.** Gear parameters of the investigated cycloid gearing are based on [22] and follow the conventions used in [30] for involute gears. All the length-related parameters are referenced in millimeters (mm). All the angle-related parameters are given in degrees (°).

| $z_1$ | $z_2$ | $a$ | $b$ | $\beta$ | $d_{Na1}$ | $d_{Na2}$ | $d_{Nf1}$ | $d_{Nf2}$ | $\delta_2$ | $\delta_1$ |
|---|---|---|---|---|---|---|---|---|---|---|
| 30 | 40 | 108.70 | 25 | 15 | 96.28 | 127.34 | 91.36 | 122.64 | 18.63 | 13.97 |

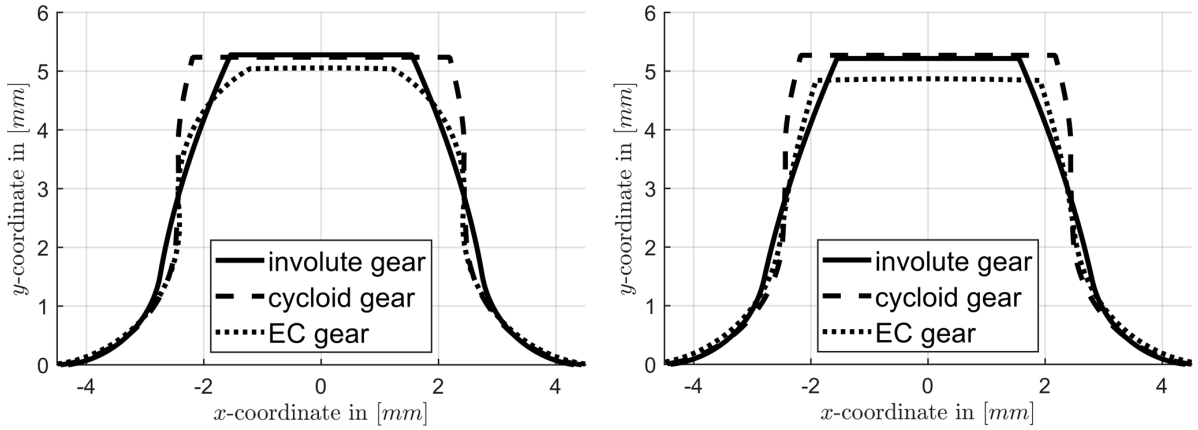



**Figure 9.** (**a**) Tooth profiles of the investigated drive pinion; (**b**) Tooth profiles of the corresponding mating gears.

The load-free and frictionless contact is analytically determined for both gearings and serves as an input. The approach by Hochrein et al. [5] is used to calculate the tooth stiffness of the uncoupled gear slices. No contact deformation is considered in the stiffness calculation, so the set of equations becomes linear. The planar normal cross-section for one contact point on the tooth profile is calculated using the proposed approach described in Section 2.2. Both gearings are discretized with 100 finite gear slices in the width direction, and 100 distinguished meshing positions on the field of contact are investigated. No premature teeth meshing is considered.

The determined load distribution of the cycloid gearing (Table 3) is depicted in Figure 10. The tooth profile is developed as a plane, and the black lines show that its boundaries and the root form radius. The black dashed line marks the start of the active profile radius. The starting point of the meshing is in the bottom left corner, and the lines of contact proceed diagonally across the tooth flank to the top right corner. The calculated line loads are in a similar range as those for the involute gearing (gearing no. 2) in Figure 7a. The single-flank engagement section can be detected in the middle of the plane. In this section, the highest line loads occur. The total contact ratio of the investigated cycloid gearing is $\varepsilon_\gamma = 1.97$, and, therefore, the single-flank engagement section is relatively small. High loads occur, even without considering boundary effects at the starting and ending points of the meshing in the bottom left and top right corners. The gear pair's stiffness at contact points in this region is similar to those in the middle of the tooth profile. When one additional tooth pair comes into contact at the end of the single-flank engagement section, the overall length of the lines of contact does not increase significantly at the beginning. The load is distributed accordingly with similar stiffnesses, and a high linear load occurs in the bottom left corner of the tooth flank. The same reasoning is valid before the second tooth pair loses contact at the beginning of the single-flank engagement section. In the dual-flank engagement section, less loaded areas on the flank occur when the lines of contact on both tooth pairs have similar lengths. This is also clearly visible in the presented load distribution.

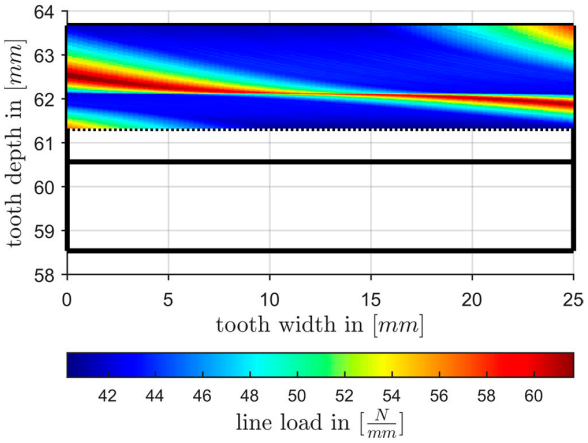



**Figure 10.** Calculated load distribution of the cycloid gear (Table 3) on the mating gear's tooth flank. The tooth profile is developed as a plane and the black lines indicate the boundaries of the tooth flank. The black dashed line marks the start of the active profile radius.

Similar to Figure 10, Figure 11 shows the obtained load distribution of the EC gearing (Table 2) on a plane representing the development of the equidistant trochoid gear's tooth, using the presented calculation approach. The black lines indicate the boundaries of the tooth profile. The contact lines at the start and end of the single-flank engagement are marked as black dashed lines. In the meshing sequence, the tooth pair comes into contact at the bottom left corner and loses contact at the top right corner. The lines of contact run diagonally across the tooth flank. The single-flank engagement section is relatively small because of a total contact ratio of $\varepsilon_\gamma = 1.99$. Near the tooth root of the EC gear, high line loads occur because of the high normal pressure angle in this region. The tooth stiffness at contact points in this region is significantly higher than at other contact points on the flank. The mating arc gear does not show a comparable increase in the tooth stiffness at contact points at the root of its active flank. Therefore, the maximum total tooth pair stiffness is shifted to the root of the equidistant trochoid gear. The highest line loads are visible in the bottom left corner of Figure 11. After the single-flank engagement section, the second tooth pair comes into contact in this region. Because of the high tooth stiffness at the root of the equidistant trochoid flank and only a slight increase in the overall length of the lines in contact at the beginning of the two tooth pairs in contact, the high load in this region is reasonable.

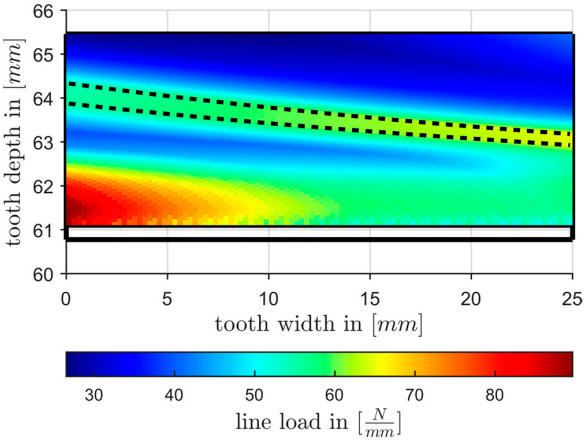



**Figure 11.** Calculated load distribution of the EC gear (Table 2) on the cycloid tooth flank. The tooth profile is developed as a plane and the black lines indicate the boundaries of the tooth flank. The contact lines at the start and end of the single-flank engagement section are marked as black dashed lines.

## 4. Conclusions

This paper suggests an analytical approach to calculate the static load distributions of non-involute conjugate gears based on modifying the established approach for involute gears. A relationship between the applied torque and the transmission error at one meshing position is derived, enabling the calculation of the line loads occurring on the tooth flank and the normal pressure. This approach is based on a load-free and frictionless contact analysis of the investigated gearing in advance. At every meshing position, the number of teeth in contact and the contact lines have to be determined, serving as input data. These contact lines are discretized, and a finite number of contact points are investigated. At each point in contact, non-load-dependent normal deviations from the ideal flank geometry can be considered. Therefore, topological micro-modifications of the tooth flank, such as axial or longitudinal crowning, can be applied, and the load distribution on the modified tooth flank can be calculated. The tooth stiffness calculation can be performed analytically or numerically, and the stiffness matrix of the discretized tooth flank at one meshing position serves as an input. In the case of an analytical stiffness calculation, a normal planar cross-section is needed. Furthermore, the paper introduces a possible definition of a normal cross-section for general non-involute tooth profiles by modifying the transverse tooth thickness at the contact point with the local helix angle and adjusting the width of the discretized gear slice.

The proposed approach is validated for involute gears, with the calculation program RIKOR, by considering two exemplary involute gearings. The tooth stiffness is calculated using the approach by Hochrein et al. [5]. The results in both cases are in good agreement with the reference solution, with deviations under an absolute value of 10%. The proposed approach is further applied to one exemplary cycloid gear and one EC gear with gear profiles and parameters similar to those of the investigated helical involute gear. The range of the determined load distribution on the tooth flanks is comparable for all three cases. The results show interesting insights into the distribution of the applied load on different gearings and demonstrate the transferability of the presented method to non-involute gears. An analytical calculation of the load distribution of non-involute gearings is, therefore, possible.

Further investigations could focus on comparing the proposed approach with a numerical finite element simulation. Therefore, implementing more sophisticated calculation approaches of the tooth stiffness is beneficial. A modification of the substitute model of a finite cantilever plate, introduced by Schmidt [8], to non-involute tooth profiles is conceivable. Based on the derived results, topological flank modifications for special gears can also be determined to adjust and equally distribute the load on tooth flanks. The authors hope this paper is a good starting point for further research.

**Author Contributions:** Conceptualization, K.F. and S.L.; methodology, K.F. and S.L.; software, K.F.; validation, K.F., S.L. and J.-F.B.; writing—original draft preparation, K.F.; writing—review and editing, S.L., J.-F.B., M.O. and K.S.; visualization, K.F.; supervision, M.O. and K.S.; project administration, K.S.; funding acquisition, K.S. All authors have read and agreed to the published version of the manuscript.

**Funding:** The presented results are based on the research project IGF no. 20549N/2 (FVA 864 I), which is supported by the German Federation of Industrial Research Associations e.V. (AiF).

**Data Availability Statement:** Data is contained within the article.

**Conflicts of Interest:** The authors declare no conflicts of interest.

## Nomenclature

**Symbols**

| | | | | | |
|---|---|---|---|---|---|
| A | Starting point of meshing | $a$ | Center distance | B | Starting point of single-flank engagement |
| $b$ | Face width | C | Pitch point | CP | Contact point |
| $c$ | Stiffness | $c^*$ | Tip clearance factor | D | Ending point of single-flank engagement |
| $d$ | Diameter | $E$ | Young's modulus | $F_b$ | Force on a finite gear slice |
| $m_n$ | Normal module | $n$ | Normal vector | $q$ | Line load |
| $r$ | Radius | $r_a^*$ | Arc radius factor | $s$ | Tooth thickness |
| $S_t^*$ | Tooth thickness factor | $T$ | Torque | $x$ | Profile shift coefficient, X-coordinate |
| $y$ | Y-coordinate | $z$ | Number of teeth, Z-coordinate | | |

**Greek symbols**

| | | | | | |
|---|---|---|---|---|---|
| $\alpha$ | Pressure angle | $\beta$ | Helix angle | $\Delta$ | Relative deviation |
| $\delta$ | Local deflection at a point on the tooth flank | $\delta^*$ | Local flank modification in the normal direction at a point on the tooth flank | $\delta_1$ | Pitch circle of the hypocycloid |
| $\delta_2$ | Pitch circle of the epicycloid | $\delta_{ges}$ | Total deflection in the plane of action | $\varepsilon_\gamma$ | Total contact ratio |
| $\lambda$ | Trochoid ratio | $\nu$ | Poisson's ratio | $\varphi_{A,s}$ | Starting angle of arc profile |
| $\varphi_{A,e}$ | Ending angle of arc profile | $\varphi_{ges}$ | Transmission error | $\varphi_j$ | Backlash angle |

**Indices**

| | | | | | |
|---|---|---|---|---|---|
| 1 | Pinion gear | 2 | Mating gear | $b$ | Base circle |
| $CP$ | Contact point | $CA$ | Calculation approach | $Na$ | Active tip |
| $Nf$ | Active root | $n$ | Normal | $RI$ | RIKOR |
| $t$ | Transverse | $y$ | Y-cylinder | | |

## References


1. *ISO 6336-1:2019-11*; Calculation of Load Capacity of Spur and Helical Gears—Part 1: Basic Principles, Introduction and General Influence Factors. ISO: Geneva, Switzerland, 2019.
2. Weber, C.; Banaschek, K. *Formänderung und Profilrücknahme bei Gerad- und Schrägverzahnten Rädern*; Schriftreihe Antriebstechnik vol. 11; Vieweg-Verlag: Braunschweig, Germany, 1953.
3. Geiser, H.; Schinagl, S. Messung der Zahnsteifigkeit eines geradverzahnten Stirnrades und Vergleich mit FEM und Berechnungen nach Weber/Banaschek. *FZG Bericht* **1996**, *Nr. 2064*, 1–52.
4. Lutz, M. Methoden zur rechnerischen Ermittlung und Optimierung von Tragbildern an Schneckengetrieben. Ph.D. Dissertation, Technical University of Munich, Munich, Germany, 2000.
5. Hochrein, J.-F.; Otto, M.; Stahl, K. Fast tooth deflection calculation method and its validation. *Forsch. Im Ingenieurwesen* **2022**, *86*, 854–859. [CrossRef]
6. *DIN 3990-1:1987-12*; Tragfähigkeitsberechnung von Stirnrädern—Einführung und allgemeine Einflußfaktoren. DIN: Berlin, Germany, 1987.
7. Niemann, G.; Winter, H. *Maschinenelemente: Band 2: Getriebe allgemein, Zahnradgetriebe—Grundlagen, Stirnradgetriebe*, 2nd ed.; Springer: Berlin/Heidelberg, Germany, 2003; ISBN 978-3-662-11874-0.
8. Schmidt, G. Berechnung der Wälzpressung Schrägverzahnter Stirnräder unter Berücksichtigung der Lastverteilung. Ph.D. Dissertation, Technical University of Munich, Munich, Germany, 1972.
9. Kunert, J.; Trempler, U.; Wikidal, F.; Senf, M.; Oster, P.; Linke, H.; Höhn, B.-R. *FVA-Nr. 224/I+II—Heft 458—Lastverteilungsmessung: Weiterentwicklung der Grundlagen zur Ermittlung der Lastaufteilung und Lastverteilung bei Außenverzahnten Gerad- und Schrägstirnrädern durch Verformungs- und Spannungsmessung*; Forschungsvereinigung Antriebstechnik e.V.: Frankfurt, Germany, 1995.
10. Schaefer, S. Verformungen und Spannungen von Kegelradverzahnungen Effizient Berechnet. Ph.D. Dissertation, Technische Universität Dresden, Dresden, Germany, 2018.
11. Wu, S.-H.; Tsai, S.-J. Contact stress analysis of skew conical involute gear drives in approximate line contact. *Mech. Mach. Theory* **2009**, *9*, 1658–1676. [CrossRef]
12. Marafona, J.D.; Marques, P.M.; Martins, R.C.; Seabra, J.H. Mesh stiffness models for cylindrical gears: A detailed review. *Mech. Mach. Theory* **2021**, *166*, 104472. [CrossRef]

13. Natali, C.; Battarra, M.; Dalpiaz, G.; Mucchi, E. A critical review on FE-based methods for mesh stiffness estimation in spur gears. *Mech. Mach. Theory* **2021**, *161*, 104319. [CrossRef]
14. Placzek, T. Lastverteilung und Flankenkorrektur in Gerad- und Schrägverzahnten Stirnradstufen. Ph.D. Dissertation, Technical University of Munich, Munich, Germany, 1988.
15. Winter, H.; Placzek, T. Load Distribution and Topological Flank Modification of Helical and Double Helical Gears. *Eur. J.* **1991**, *36*, 171–176.
16. Weinberger, U.; Otto, M.K.; Stahl, K. Closed-Form Calculation of Lead Flank Modification Proposal for Spur and Helical Gear Stages. *J. Mech. Des.* **2020**, *142*, 031106. [CrossRef]
17. Daffner, M. Validierung von Verformungsberechnungen im System Zahnrad-Welle-Lager-Gehäuse. Ph.D. Dissertation, Technical University of Munich, Munich, Germany, 2017.
18. Gu, L.; Xu, J.; Luo, S. The Design of New Cycloid Gear with Variable Cross Section and the Research of End Milling in Five-Axis Machine Tool. *Manuf. Technol.* **2016**, *3*, 497–502. [CrossRef]
19. Baciu, I.; Vasilescu, A.-G.; Avram, M.; Gramescu, B.; Constantin, V.; Moraru, E. A Review of Additive Technologies Applied to Gear Transmission. In *Innovations in Mechanical Engineering III. icieng 2024*; Machado, J., Soares, F., Trojanowska, J., Ottaviano, E., Valášek, P., Reddy, D.M., Perondi, E.A., Basova, Y., Eds.; Springer Nature: Cham, Switzerland, 2024; pp. 44–55, ISBN 978-3-031-62684-5.
20. Johann, A.; Scheurle, J. On the generation of conjugate flanks for arbitrary gear geometries. *GAMM* **2009**, *1*, 61–79. [CrossRef]
21. Römhild, I.; Linke, H. *FVA-Nr. T 492—Heft 436—Sonderprofile: Evolventische und Nichtevolventische Sonderverzahnungen -Studie-*; Forschungsvereinigung Antriebstechnik e.V.: Frankfurt, Germany, 1994.
22. Lehmann, M. Die Beschreibung der Zykloiden, ihrer Äquidistanten und Hüllkurven: Unter besonderer Berücksichtigung der Planeten-Getriebe mit Zykloiden-Kurvenscheiben. Habilitation Thesis, Technical University of Munich, Munich, Germany, 1981.
23. Landler, S.; Trübswetter, M.; Otto, M.; Stahl, K. Parameter based definition of ecentric cycloid gearings. *Forsch. Im Ingenieurwesen* **2023**, *87*, 807–819. [CrossRef]
24. Kazakyavichyus, S.M.; Stanovskoy, V.V.; Remneva, T.A.; Kuznetsov, V.M.; Bubenchikov, A.M.; Shcherbakov, N.R. Performance of eccentric-cycloid engagement with change in the interaxial distance: Modification of tooth configuration. *Russ. Eng. Res.* **2011**, *3*, 197–199. [CrossRef]
25. Li, X.; Li, C.; Chen, B.; Liang, D. Design and investigation of a cycloid helical gear drive. *J. Mech. Sci. Technol.* **2017**, *9*, 4329–4336. [CrossRef]
26. Batsch, M.; Wydrzyński, D.; Przeszłowski, Ł. Tooth Contact Analysis of Cylindrical Gears with an Unconventional Tooth Profile. *Adv. Sci. Technol. Res. J.* **2022**, *4*, 119–129. [CrossRef]
27. Bubenchikov, A.M.; Kazakavitschyus, S.M.; Shcherbakov, N.R. Mathematical simulation of a profile cutter as a surface of revolution. *IOP Conf. Ser. Mater. Sci. Eng.* **2016**, *124*, 12095. [CrossRef]
28. Batsch, M. Rapid Prototyping and Tooth Contact Analysis of Eccentric Cycloid Gear Mesh. *J. KONBiN* **2019**, *1*, 369–382. [CrossRef]
29. Linke, H.; Börner, J.; Heß, R. *Cylindrical Gears: Calculation—Materials—Manufacturing*, 1st ed.; Carl Hanser Verlag: Munich, Germany, 2016; ISBN 978-1-56990-489-3.
30. *DIN ISO 21771:2014-08*; Zahnräder—Zylinderräder und Zylinderradpaare mit Evolventenverzahnung—Begriffe und Geometrie. DIN: Berlin, Germany, 2014.
31. Otto, M. Lastverteilung und Zahnradtragfähigkeit von schrägverzahnten Stirnrädern. Ph.D. Dissertation, Technical University of Munich, Munich, Germany, 2009.


**Disclaimer/Publisher's Note:** The statements, opinions and data contained in all publications are solely those of the individual author(s) and contributor(s) and not of MDPI and/or the editor(s). MDPI and/or the editor(s) disclaim responsibility for any injury to people or property resulting from any ideas, methods, instructions or products referred to in the content.